

# Stability of pressure-driven creeping flows in channels lined with a nonlinear elastic solid

By VASILEIOS GKANIS AND SATISH KUMAR

Department of Chemical Engineering and Materials Science, University of Minnesota,  
151 Amundson Hall, 421 Washington Avenue SE, Minneapolis, MN 55455, USA

(Received 22 January 2004 and in revised form 20 September 2004)

The effect of pressure gradients on the stability of creeping flows of Newtonian fluids in channels lined with an incompressible and impermeable neo-Hookean material is examined in this work. Three different configurations are considered: (i) pressure-driven flow between a rigid wall and a wall lined with a neo-Hookean material; (ii) pressure-driven flow between neo-Hookean-lined walls; and (iii) combined Couette–Poiseuille flow between a rigid wall and a neo-Hookean-lined wall. In each case, a first normal stress difference whose magnitude depends on depth arises in the base state for the solid, and linear stability analysis reveals that this leads to a short-wave instability which is removed by the presence of interfacial tension. For sufficiently thick solids, low-wavenumber modes become unstable first as the applied strain increases above a critical value, whereas for sufficiently thin solids, high-wavenumber modes becomes unstable first. Comparison of the dimensionless critical strains shows that configurations (i) and (ii) are more difficult to destabilize than Couette flow past a neo-Hookean solid. For configuration (iii), the nonlinear elasticity of the solid leads to two physically distinct critical conditions, in contrast to what happens when a linear elastic material is used. The mechanisms underlying the behaviour of the critical strains are explained through an analysis of the interfacial boundary conditions.

---

## 1. Introduction

In contrast to rigid boundaries, flexible solid boundaries can deform under the action of shear and normal stresses, resulting in the creation of surface waves. If the stresses are exerted by an adjacent flowing fluid, these waves may lead to a complicated, time-dependent flow. Important consequences of this modified flow include the alteration of mass and heat transfer rates and alteration of the stresses exerted on the solid surface. Such elasto-hydrodynamic instabilities, if better understood, could find application in a variety of areas including microfluidic mixers, membrane separations and the rheology of complex fluids that undergo flow-induced gelation. Most prior work on elasto-hydrodynamic instabilities has modelled the solid as a linear viscoelastic material, which tacitly assumes that the deformation gradients in the solid are small. However, large deformations of the solid can give rise to normal stress phenomena, which may considerably influence instability behaviour. In order to understand better the role of large deformations and normal stresses, we study here the stability of pressure-driven creeping flows of Newtonian fluids in channels lined with a neo-Hookean material.

The stability of creeping plane Couette flow past a linear viscoelastic solid was studied by Kumaran, Fredrickson & Pincus (1994), who found that interfacial waves

become unstable beyond a critical dimensionless strain  $\Gamma = \mu V / (RE)$ , where  $\mu$  is the fluid viscosity,  $V$  is the speed of the surface driving the motion,  $R$  is the fluid thickness and  $E$  is the shear modulus of the solid. This critical value depends on the fluid-to-solid thickness ratio, interfacial tension and viscosity ratio. Gkanis & Kumar (2003) examined the role of large deformations by using instead a neo-Hookean model, which is one of the simplest nonlinear constitutive laws for solids. They found that in contrast to the linear viscoelastic model, a first normal stress difference develops in the base state. This has a dramatic impact on instability behaviour as it gives rise to a short-wave instability that becomes pronounced for solid-to-fluid thickness ratios of  $O(1)$  or smaller. In addition, it leads to values of the critical strain that are smaller than those for the linear viscoelastic model.

In the case of creeping plane Couette flow past a linear viscoelastic solid, the only coupling between the base state and the perturbation variables occurs through the continuity of velocity boundary condition at the interface and involves the velocity gradient of the mean flow. Thus, once the Couette problem has been solved, it is trivial to obtain the results for plane Poiseuille flow; we simply have to evaluate the interfacial value of the base-state velocity gradient associated with a given applied pressure gradient. The same is not true for plane Couette flow past a neo-Hookean solid. Here, the coupling between the base state and the perturbation variables occurs through the governing equations and continuity of stress boundary condition as well, and involves also the base-state values of the first normal stress difference and deformation gradient in the solid. These base-state values are independent of position for Couette flow, but they vary with depth for plane Poiseuille flow. This gives rise to an eigenvalue problem with variable coefficients (whereas for plane Couette flow the coefficients are constant), and as a consequence, it is no longer trivial to determine the results for Poiseuille flow from the Couette solution.

To elucidate the role of normal stress phenomena on the stability of pressure-driven flows past deformable solids, we consider here three problems in the creeping-flow limit: (i) pressure-driven flow between a rigid wall and a wall lined with a neo-Hookean material; (ii) pressure-driven flow between neo-Hookean-lined walls; and (iii) combined Couette–Poiseuille flow between a rigid wall and a neo-Hookean-lined wall. Linear stability analysis is applied to determine the relative stability of these flows, and the results are rationalized on the basis of differences in interfacial boundary conditions.

Before proceeding, we briefly review some related work in order to place our contribution in a proper context. Experiments in which a viscous fluid was placed on a polymer gel in a parallel-plate rheometer were performed to test the theoretical predictions of Kumaran *et al.* (1994) (Kumaran & Muralikrishnan 2000; Muralikrishnan & Kumaran 2001). A sharp increase in the apparent viscosity was observed above a critical strain rate, and the critical value was predicted well by the theory. Because the solid-to-fluid thickness ratio in these experiments was sufficiently large, the deformation gradients in the solid were relatively small at the instability onset, so the use of a linear constitutive model for the solid would be expected to work well (Gkanis & Kumar 2003). Eggert & Kumar (2004) carried out similar experiments on a different fluid–gel system and also saw a sharp increase in the apparent viscosity. In addition, they probed the nonlinear characteristics of the instability and found evidence of subcritical behaviour, consistent with predictions of a weakly nonlinear analysis (Shankar & Kumaran 2001).

The effects of fluid inertia on instability of plane Couette flow past a linear viscoelastic solid have been analysed by Srivatsan & Kumaran (1997), who found

that the critical Reynolds number for instability increases with the ratio of the momentum diffusion time to the elastic relaxation time. The role of fluid elasticity in the creeping flow limit was considered by Shankar & Kumar (2003), who used an upper-convected Maxwell model. They found that the presence of fluid elasticity has a stabilizing effect, and that there is a single unstable mode which reverts to the mode of Kumaran *et al.* (1994) when the fluid is Newtonian and the well-known Gorodtsov–Leonov (Gorodtsov & Leonov 1967) mode when the solid is rigid.

The stability of pressure-driven flows through cylindrical tubes lined with a layer of a linear viscoelastic material has been extensively studied. At low-to-moderate Reynolds numbers, the flow is found to be unstable to axisymmetric disturbances (Kumaran 1995; 1998), and at very large Reynolds numbers, non-axisymmetric modes may be even more unstable than axisymmetric ones (Shankar & Kumaran 2000; Hamadiche & Gad-el-Hak 2002). Related experiments were conducted by Krindel & Silberberg (1979), who observed that the transition from a laminar flow to a turbulent flow in a gel-lined tube occurs at a much lower Reynolds number than for a rigid-walled tube. Although this observation appears to be consistent with the instability mechanism proposed by Kumaran (1998), a conclusive comparison between theory and experiment could not be made. The stability of pressure-driven flows through a planar channel lined with a linear elastic solid was investigated by Pierucci & Morales (1990). For sufficiently low Reynolds numbers, they found that wall compliance (as measured by the transverse wave speed) has a destabilizing effect, whereas stabilization was observed for sufficiently large Reynolds numbers.

Also related to the present work are numerous studies on the use of flexible surfaces to inhibit boundary-layer instabilities (Carpenter, Lucey & Davies 2001; Gad-el-Hak 2003). Both theory and experiment indicate that surface deformability can reduce the growth rates of Tollmein–Schlichting waves, but also reveal that new modes of instability may be introduced. These new modes arise owing to the ability of waves to propagate at the fluid–solid interface, and are often referred to as a flow-induced surface instability (FISI). The instability studied here is an example of a FISI since it would not exist if the boundaries were rigid. In the modelling of boundary-layer instabilities near flexible surfaces, the solid has typically been described as a thin spring-backed membrane whose deflection is governed by a linear equation or as a finite-thickness linear viscoelastic solid. Similar models have also been applied to examine the stability of pressure-driven flows between flexible surfaces in order to shed light on the boundary-layer instabilities discussed above (Davies & Carpenter 1997). Apart from drag reduction applications, instability of turbulent airflow over a linear viscoelastic solid has been studied as a model of mucus clearance in the lungs (Moriarty & Grotberg 1999).

The organization of this paper is as follows. The governing equations are presented in §2, the base states are calculated in §3, and the linear stability analysis is detailed in §4. In §5, we present the results from our analysis, and in §6 we probe the mechanisms underlying the behaviour we observe. The conclusions are given in §7.

## 2. Governing equations

We consider an incompressible Newtonian fluid residing on top of an incompressible and impermeable neo-Hookean solid (figure 1). The interface between the fluid and solid is flat and located at  $z = 0$  in the base state. In the case of pressure-driven flow between a rigid wall and a neo-Hookean material (hereinafter referred to as Poiseuille flow past a neo-Hookean solid), a rigid stationary plate is located at  $z = R$ . For

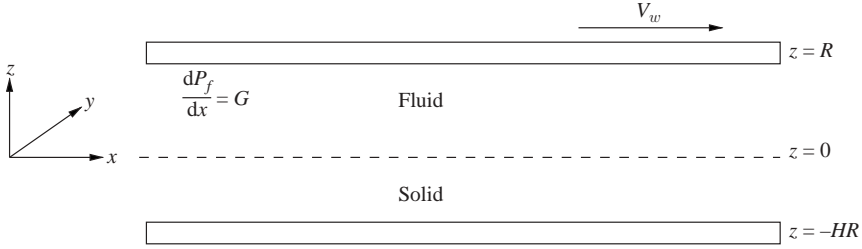


FIGURE 1. Problem geometry. In the case of Poiseuille flow in a deformable channel, the top plate is replaced by a line of symmetry.

combined Couette–Poiseuille flow, the plate moves with a velocity  $\mathbf{v} = V_w \mathbf{i}$ , where  $\mathbf{i}$  is the unit vector in the  $x$ -direction. For pressure-driven flow between neo-Hookean-lined walls (hereinafter referred to as Poiseuille flow in a deformable channel), symmetry rather than no-slip boundary conditions are applied at  $z = R$ . In all cases, the solid is attached to a stationary rigid plate at  $z = -HR$  and a constant pressure gradient in the  $x$ -direction is applied to the fluid. As have prior works (Kumaran *et al.* 1994; Gkanis & Kumar 2003), we focus our efforts here on two-dimensional systems and suppress any variations in the  $y$ -direction.

We present the governing equations in dimensionless form, where the length has been scaled by  $R$ , time by  $\mu_f/E$ , and pressure by  $E$ , in which  $\mu$  is the fluid viscosity and  $E$  is the shear modulus of the solid. The motion of the fluid is governed by Stokes' equations:

$$\nabla \cdot \mathbf{v} = 0, \quad (2.1)$$

$$-\nabla P_f + \nabla^2 \mathbf{v} = 0, \quad (2.2)$$

where  $P_f$  is the dynamic pressure of the fluid. The deformation of the solid is governed by:

$$\det(\mathbf{F}) = 1, \quad (2.3)$$

$$\nabla_x \cdot \mathbf{P} = 0, \quad (2.4)$$

where  $\mathbf{F}$  is the deformation gradient tensor and  $\mathbf{P}$  is the first Piola–Kirchhoff stress tensor, which is related to the Cauchy stress tensor,  $\boldsymbol{\tau}$ , through the equation (Malvern 1969):

$$\mathbf{P} = \mathbf{F}^{-1} \cdot \boldsymbol{\tau}. \quad (2.5)$$

Inertial effects have been neglected in the above equations by considering the limit  $Re = \rho_f ER^2/\mu_f^2 \ll 1$ , where  $\rho_f$  is the fluid density, and assuming that the fluid and solid densities are comparable.

The governing equations for the fluid are written in the current configuration, whereas the governing equations for the solid are written in the reference configuration. For the solid, we are using capital letters with subscripts  $\mathbf{X} = (X_1, X_2, X_3)$  to denote the spatial coordinates  $(x, y, z)$  in the reference configuration, and lower-case letters with subscripts  $\mathbf{x} = (x_1, x_2, x_3)$  to denote the spatial coordinates in the current configuration. For the fluid, we adopt the  $(x, y, z)$  coordinate system, which coincides with the reference coordinate system  $(X_1, X_2, X_3)$  used for the solid. The subscript  $X$  in (2.4) indicates differentiation in the reference configuration, and the deformation gradient tensor is given by  $\mathbf{F} = \nabla_x \mathbf{x}$ .

There are a number of constitutive equations for isotropic solid materials that satisfy the principle of material frame indifference. Among these, we use the neo-Hookean model because it is the simplest nonlinear constitutive equation and because it is used to describe the behaviour of model elastomers (Macosko 1994). The dimensionless Cauchy stress tensor for the neo-Hookean material is given by the equation:

$$\boldsymbol{\tau} = -P_s \mathbf{I} + \mathbf{F} \cdot \mathbf{F}^T, \tag{2.6}$$

where  $P_s$  is a pressure-like function which is related to the pressure in the solid,  $P$ , through the dimensionless equation  $P_s = P - 1$ . We note that the neo-Hookean model is purely elastic and does not contain a viscous component.

Equations (2.1)–(2.6) form a system of nonlinear partial differential equations which are subject to the following boundary conditions. At the bottom plate, there is no displacement:

$$\mathbf{x} = \mathbf{X} \quad \text{at} \quad z = -H. \tag{2.7}$$

At the top plate,  $z = 1$ , the boundary conditions depend on the problem under consideration. For Poiseuille flow past a neo-Hookean solid, we have:

$$\mathbf{v} = 0, \tag{2.8}$$

whereas for combined Couette–Poiseuille flow:

$$\mathbf{v} = G_1 \mathbf{i}. \tag{2.9}$$

Here,  $G_1 = \mu V_w / (RE)$  and can be interpreted as a dimensionless imposed velocity or strain. For Poiseuille flow in a deformable channel, we apply the symmetry conditions:

$$v_z = 0, \tag{2.10}$$

$$\frac{\partial v_x}{\partial z} = 0. \tag{2.11}$$

At the solid–fluid interface, continuity of velocities and forces holds:

$$\mathbf{v} = \frac{\partial \mathbf{x}}{\partial t}, \tag{2.12}$$

$$\mathbf{n} \cdot \boldsymbol{\tau} = \mathbf{n} \cdot \boldsymbol{\sigma} + nT\kappa, \tag{2.13}$$

where  $\mathbf{n}$  is the normal vector to the interface,  $T$  is the scaled interfacial tension,  $T = \gamma / (ER)$ , in which  $\gamma$  is the dimensional interfacial tension and  $\kappa$  is the curvature. The Cauchy stress tensors for the solid and the fluid are  $\boldsymbol{\tau}$  and  $\boldsymbol{\sigma}$ , respectively.

### 3. Base states

In the base state, continuity of velocity, (2.12), simplifies to  $\mathbf{v} = 0$  (steady state) and continuity of forces, (2.13), takes the form  $\mathbf{k} \cdot \boldsymbol{\tau} = \mathbf{k} \cdot \boldsymbol{\sigma}$ , where  $\mathbf{k}$  is the unit vector in the  $z$ -direction. We now give the base state for each of the problems that we are studying.

#### 3.1. Poiseuille flow past a neo-Hookean solid

Under the action of a constant pressure gradient and no-slip boundary conditions at the top plate and the interface, a Poiseuille flow develops in the fluid:

$$v_x = \frac{1}{2}G(z^2 - z), \tag{3.1}$$

$$v_z = 0, \tag{3.2}$$

$$P_f = P_f(x), \tag{3.3}$$

where  $G = (R/E)\partial P_f^*/\partial x^*$  with  $\partial P_f^*/\partial x^*$  representing the dimensional imposed pressure gradient. Then, for the dimensionless pressure we have  $P_f(x) = Gx + C_0$ , where  $C_0$  is a constant.

The displacement and pressure in the solid are given by the following equations:

$$x_1 = X_1 + \frac{1}{2}G(X_3^2 - H^2) - \frac{1}{2}G(X_3 + H), \quad (3.4)$$

$$x_3 = X_3, \quad (3.5)$$

$$P_s = P_f(X_1) + 1 + \frac{1}{2}G^2(X_3^2 - X_3). \quad (3.6)$$

In addition, there is a first normal stress difference in the solid:

$$\tau_{11} - \tau_{33} = (GX_3 - \frac{1}{2}G)^2. \quad (3.7)$$

### 3.2. Poiseuille flow in a deformable channel

The symmetric boundary conditions at the top plate slightly change the base state of the previous problem:

$$v_x = G\left(\frac{1}{2}z^2 - z\right), \quad (3.8)$$

$$v_z = 0, \quad (3.9)$$

$$P_f = P_f(x), \quad (3.10)$$

for the fluid, and:

$$x_1 = X_1 + \frac{1}{2}G(X_3^2 - H^2) - G(X_3 + H), \quad (3.11)$$

$$x_3 = X_3, \quad (3.12)$$

$$P_s = P_f(X_1) + 1 + G^2\left(\frac{1}{2}X_3^2 - X_3\right), \quad (3.13)$$

for the solid, with:

$$\tau_{11} - \tau_{33} = (GX_3 - G)^2. \quad (3.14)$$

### 3.3. Combined Couette–Poiseuille flow

In this case, a Couette–Poiseuille flow develops in the fluid:

$$v_x = \frac{1}{2}Gz^2 + \beta z, \quad (3.15)$$

$$v_z = 0, \quad (3.16)$$

$$P_f = P_f(x), \quad (3.17)$$

where  $\beta = G_1 - G/2$ . The displacement and pressure in the solid are given by the equations:

$$x_1 = X_1 + \frac{1}{2}G(X_3^2 - H^2) + \beta(X_3 + H), \quad (3.18)$$

$$x_3 = X_3, \quad (3.19)$$

$$P_s = P_f(X_1) + 1 + \frac{1}{2}G^2X_3^2 + \beta GX_3. \quad (3.20)$$

The corresponding first normal stress difference is:

$$\tau_{11} - \tau_{33} = (GX_3 + \beta)^2. \quad (3.21)$$

### 3.4. Remarks

The system is set in motion by the application of a constant pressure gradient,  $G$ . Because of the choice of the coordinate system,  $G$  will always be negative so that there is a flow in the positive  $x$ -direction. In the problem of combined Couette–Poiseuille

flow, two forces are exerted on the system: the first is the pressure gradient, whose value is chosen explicitly from the parameter  $G$ , and the second force is the shear stress from the top plate, whose value is set by the parameter  $\beta$ . Again, we choose  $G$  to be negative (to be consistent with the other two problems), but the sign of  $\beta$  can be positive (or negative) allowing for the development of a Couette flow to the right (or left). Here, we note that from the equations for the combined Couette–Poiseuille flow, (3.15)–(3.20), we can recover the equations for the Poiseuille flow, (3.1)–(3.6), by setting  $\beta = 0$ , and the equations for the Couette flow by setting  $G = 0$ .

From (3.6), (3.13) and (3.20), we observe that the pressure in the solid increases with depth. This is a consequence of having a first normal stress difference whose magnitude is depth-dependent. This was not observed in the problem of Couette flow past a neo-Hookean solid (Gkanis & Kumar 2003), where the pressure in the solid was constant and equal to the pressure in the fluid. In that problem, the first normal stress difference in the solid is equal to  $G_1^2$ . Because there is a first normal stress difference in the solid and not in the fluid, the jump of this quantity across the interface produces a short-wave instability similar to that seen for fluid–fluid interfaces (Renardy 1988; Chen 1991). Such an instability was observed by Gkanis & Kumar (2003) and is expected here also.

#### 4. Linear stability analysis

We conduct a linear stability analysis using the standard normal mode decomposition:

$$f' = \tilde{f}(z)\exp(ikx + \alpha t), \quad (4.1)$$

where  $f'$  is the disturbance of a field variable,  $\tilde{f}(z)$  is the complex-valued amplitude (or eigenfunction),  $k$  is the real-valued wavenumber, and  $\alpha$  is the complex-valued growth rate. For the solid,  $x$  and  $z$  should be replaced by  $X_1$  and  $X_3$ , respectively. The linearized governing equations and boundary conditions for each of the problems we study are given in the Appendix.

In each problem, the governing equations for the fluid can be combined into a linear, fourth-order constant-coefficient ordinary differential equation (ODE) for  $\tilde{v}_z$  that can be solved analytically. Two of the four unknown constants in the analytical solution can be eliminated by using the boundary conditions at  $z = 1$ . Similarly for the solid, we can obtain a linear fourth-order ODE for  $\tilde{x}_3$  in each of the above problems. However, the coefficients are not constant so these equations are solved numerically. A fifth-order Runge–Kutta method is used to integrate the ODE for  $\tilde{x}_3$  from the bottom plate to the interface. Four boundary conditions at the bottom plate are required and two of them are known, (A 7). For the other two, we pick values for the second and the third derivative of  $\tilde{x}_3$  so that we have a set of two orthonormal initial conditions (Davey 1973; Mack 1976; Ho & Denn 1977). Once the interfacial values of the eigenfunctions for each initial condition are obtained, a linear combination of them involving two unknown constants is inserted into the interfacial boundary conditions (Srivatsan & Kumaran 1997). Hence, we obtain a system of four equations with four unknowns written as  $\mathbf{A}\mathbf{x} = 0$ , where  $\mathbf{x}$  is the vector of the unknown constants and  $\mathbf{A}$  is a  $4 \times 4$  matrix. Because we are not interested in the trivial solution, the determinant of  $\mathbf{A}$  must be zero, which leads to a quadratic dispersion equation whose solution gives the growth rate as a function of the thickness ratio,  $H$ , the interfacial tension,  $T$ , the wavenumber,  $k$ , and the imposed strains  $G$  and  $\beta$ . If the real part of the growth rate is positive the system is

unstable, if it is negative the system is stable, and if it is zero the system is neutrally stable. In solving the quadratic dispersion equation, we have found that one of the roots may obtain a zero or positive real part depending on the problem parameters, whereas the other root always (for the cases we have checked) has a negative real part.

We also note that in contrast to linear elastic solids, the coupling between the base state and perturbation variables occurs in several places. For linear elastic solids, that coupling occurs only in the continuity of velocity boundary condition and involves the velocity gradient of the mean flow. For neo-Hookean solids, the coupling also occurs through the governing equations in the solid and the interfacial stress balance, and involves the base-state values of the first normal stress difference and deformation gradient in the solid. Because the base states for Couette and Poiseuille flows past a neo-Hookean solid are significantly different (see §3.4), the results for Poiseuille flow cannot be obtained simply by solving the Couette problem.

## 5. Results

We begin by discussing some general features of the growth rate curves,  $\text{Re}(\alpha)$  versus  $k$ . Plots are shown for the case of Poiseuille flow past a neo-Hookean solid, but similar behaviour is observed for the other problems we study. Figure 2 shows growth rate curves for  $H = 20$ ,  $T = 0$ , and several different values of  $G$ . As  $G$  increases in magnitude, a small band of low-wavenumber modes crosses the  $x$ -axis and becomes unstable. Although the growth rate continues to decrease with  $k$  for a while beyond the cutoff wavenumber, it increases and then appears to plateau for sufficiently large  $k$ . A similar plateau was seen in the work of Gkanis & Kumar (2003), and it arises due to the jump in the first normal stress difference across the interface, which can drive a short-wave instability. For non-zero  $T$ , the plateau disappears since interfacial tension damps the short-wave disturbances. This produces a high-wavenumber hump in the growth rate curve which can become unstable even before the low-wavenumber modes if  $H$  is sufficiently small. An example of this is shown in figure 3, where  $H = 4$  and  $T = 10$ . From the above observations, we see that thick (large  $H$ ) and thin (small  $H$ ) solids behave qualitatively differently when the nonlinear elasticity of the solid is accounted for. For thick solids, low-wavenumber modes become unstable first as the applied strain is increased, whereas for thin solids high-wavenumber modes are destabilized first.

The behaviour of the growth rate curves is shown in figure 4, where we plot the critical strain,  $G_c$ , and wavenumber,  $k_c$ , for four different systems when  $T = 10$ : (i) Couette flow past a neo-Hookean solid; (ii) Couette flow past a linear elastic solid; (iii) Poiseuille flow past a neo-Hookean solid; and (iv) Poiseuille flow in a deformable channel. Here,  $G$  actually represents  $G_1$  for Couette flow; for Poiseuille flow,  $G$  has been made positive in order to ease the comparison with the Couette results. For the neo-Hookean systems,  $k_c$  jumps from a small to a large value at a critical value of  $H$ ; this is the point where the high-wavenumber modes become more unstable than the low-wavenumber modes. At this same value of  $H$ ,  $G_c$  increases sharply (but continuously) for the Poiseuille flows. A jump in  $k_c$  is also seen for Couette flows at a critical value of  $H$  (Gkanis & Kumar 2003), but  $G_c$  does not change as abruptly as for the Poiseuille flows. In all of the neo-Hookean systems,  $G_c$  appears to plateau as  $H$  decreases; this is also true for the linear elastic system, but the plateau occurs beyond the range of the plot. Finally, we note that Couette flow past a neo-Hookean solid is the easiest system to destabilize, whereas Poiseuille flow past a neo-Hookean



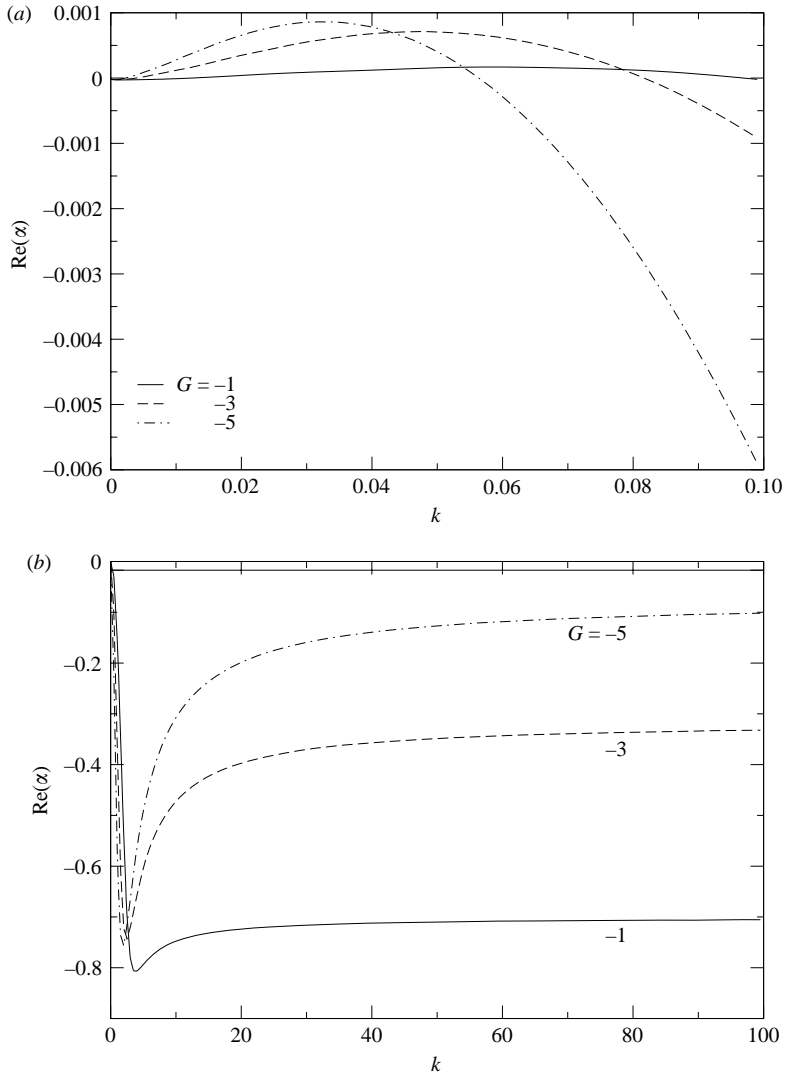


FIGURE 2. Growth rate curves for Poiseuille flow past a neo-Hookean solid when  $H = 20$  and  $T = 0$ . In (a), we have focused in on the region  $0 < k < 0.1$ . Here,  $G_c = -0.47$  and  $k_c = 0.044$ .

solid is the most difficult to destabilize for  $H < 7$  or  $H > 20$ . For values of  $H$  between these limits, Poiseuille flow in a deformable channel is the most difficult system to destabilize.

From figure 4, we observe that  $G_c$  tends to decrease as  $H$  increases. Since the first normal stress difference is proportional to  $G^2$ , its effects become pronounced for sufficiently small solid thicknesses. For sufficiently large solid thicknesses, normal stress effects will become insignificant and the results for the neo-Hookean systems should converge to the corresponding results for flow past a linear elastic solid. We have performed additional calculations in order to verify this and found that there is indeed convergence at large  $H$ . We have also examined the effects of interfacial tension: increasing  $T$  tends to increase  $G_c$  and decrease  $k_c$ , as it does in the case of Couette flow past a neo-Hookean solid (Gkanis & Kumar 2003). In addition, it tends

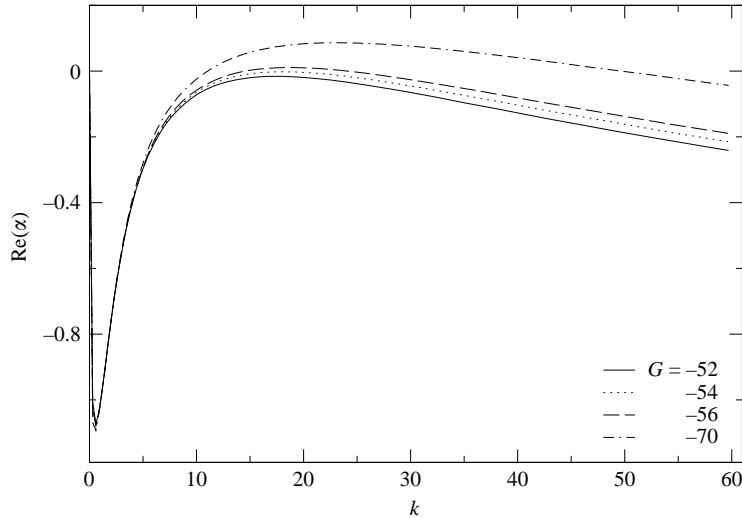


FIGURE 3. Growth rate curves for Poiseuille flow past a neo-Hookean solid when  $H=4$  and  $T=10$ . A band of high-wavenumber modes becomes unstable before a band of low-wavenumber modes (not shown) does. Here,  $G_c = -54.3$  and  $k_c = 18.2$ .

to decrease the value of  $H$  at which the transition from thick to thin solids occurs. Finally, we have observed that the imaginary part of the growth rate tends to behave as it does for Couette flow past a neo-Hookean solid (Gkanis & Kumar 2003). For relatively thick solids, it is negative at the critical conditions, whereas for relatively thin solids, it is positive. The imaginary part of the growth rate can take on positive values at high wavenumbers, and it is precisely those high-wavenumber modes that become destabilized when the solid is relatively thin. Thus, the most unstable mode will travel downstream for thick solids but upstream for thin solids. For linear elastic solids, the imaginary part of  $\alpha$  is always found to be negative.

We now turn to the results for combined Couette–Poiseuille flow. For the case where we have a linear elastic solid, the stability of this system depends on only one parameter,  $\beta$  (the velocity gradient at the interface), since the only coupling between the base state and the perturbation variables occurs through the continuity of velocity boundary condition. This will give rise to two physically equivalent critical strains,  $\pm\beta_c$ , and a single critical wavenumber. In contrast, the stability of the corresponding neo-Hookean system depends on two parameters,  $G$  and  $\beta$ . For any given value of  $G$  and other problem parameters, there will be a positive and a negative value of  $\beta$  at which the system becomes unstable. However, the nonlinear elasticity of the solid breaks the symmetry of this system so that the two values of  $\beta$  have different magnitudes as well as signs. Furthermore, the corresponding critical wavenumbers will be different.

This symmetry breaking is evident in figure 5, which shows plots of  $\beta_c$  and  $k_c$  versus  $H$  when  $T=10$  for different values of  $G$ . If  $\beta$  is positive, then an increase in the magnitude of the imposed pressure gradient causes  $\beta_c$  to increase in magnitude. If  $\beta$  is negative, this trend holds for  $H > 2$ , but for  $H < 2$  the reverse is true. Since in an experiment one would actually control the values of the pressure gradient,  $G$ , and the velocity,  $G_1$ , it is instructive to construct a stability diagram in the  $G$ – $G_1$  plane as is done in figure 6. Here, we choose two different values of  $H$ , set  $T=10$ , and

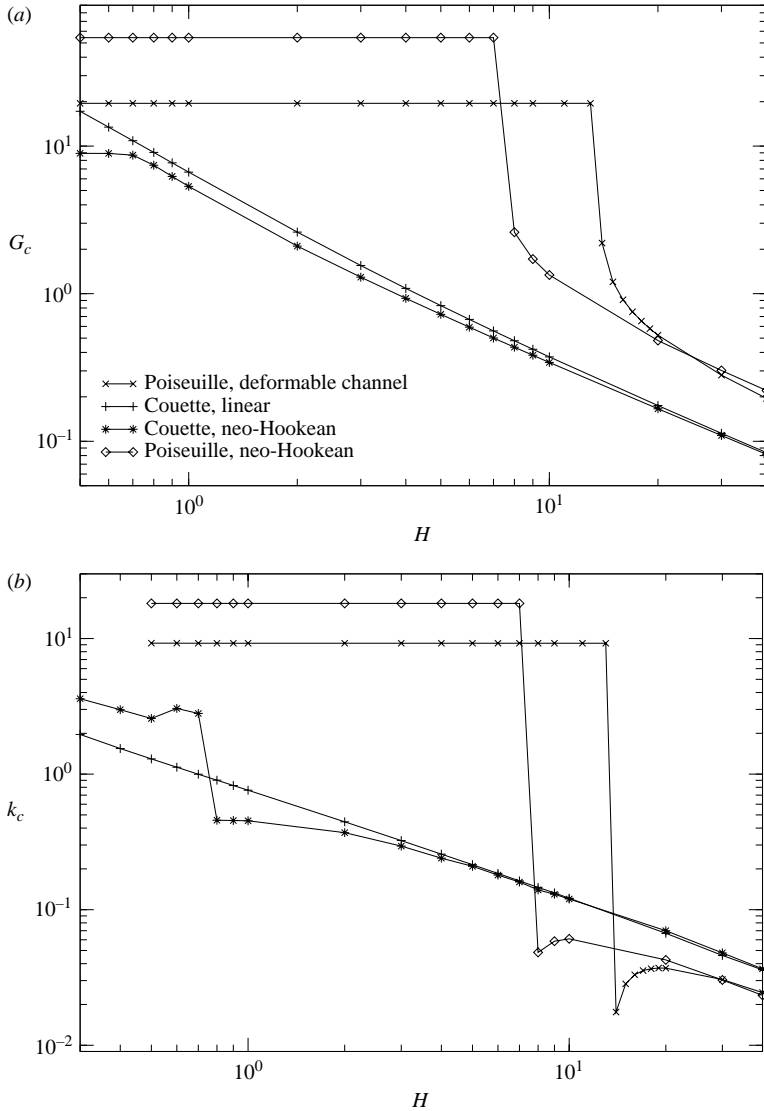


FIGURE 4. Critical value of the imposed strain,  $G_c$ , and the corresponding critical wavenumber,  $k_c$ , as a function of the thickness ratio,  $H$ , when  $T = 10$ .

show results for both neo-Hookean and linear elastic systems. It is clear from these plots that the stability window for the neo-Hookean material widens as the pressure gradient increases; for the linear elastic solid, the width of the stability window is independent of  $G$ . We also see that at a given value of  $G$ , the stability window is wider for the neo-Hookean material; this is a consequence of the interfacial boundary conditions, which we discuss in §6.4. However, if  $H$  and  $G$  are sufficiently small, the neo-Hookean window is actually narrower (figure 6a). This is consistent with the observation in figure 4 that Couette flow past a neo-Hookean solid is more unstable than Couette flow past a linear elastic solid, and that the difference diminishes as  $H$  increases.

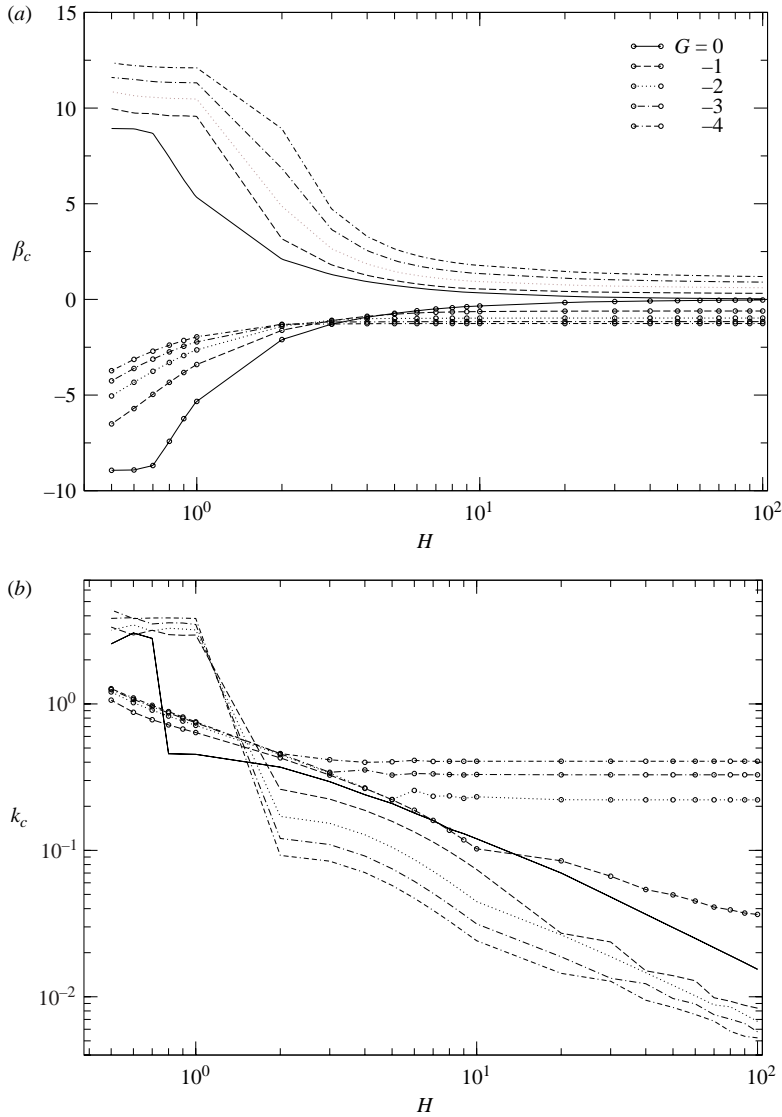


FIGURE 5. The critical value of the strain,  $\beta_c$ , and the corresponding critical wavenumber,  $k_c$ , for combined Couette–Poiseuille flow as a function of the thickness ratio,  $H$ , for different values of  $G$  when  $T = 10$ .

## 6. Mechanisms

In this section, we discuss the physical mechanisms underlying the behaviour reported in §5. The mechanism responsible for the instability was discussed in Gkanis & Kumar (2003), where it was shown that at the critical conditions, the mean flow acts to amplify horizontal perturbations to the interface while the horizontal velocity perturbations tend to suppress them. This can be deduced from the velocity boundary condition at the interface, and implies that at the critical conditions, the horizontal interface perturbations tend to be in phase with the mean flow and out of phase with the horizontal velocity perturbations. What has not yet been explained is the relative stability of the different systems considered in figure 4, e.g. why, for Couette flow,

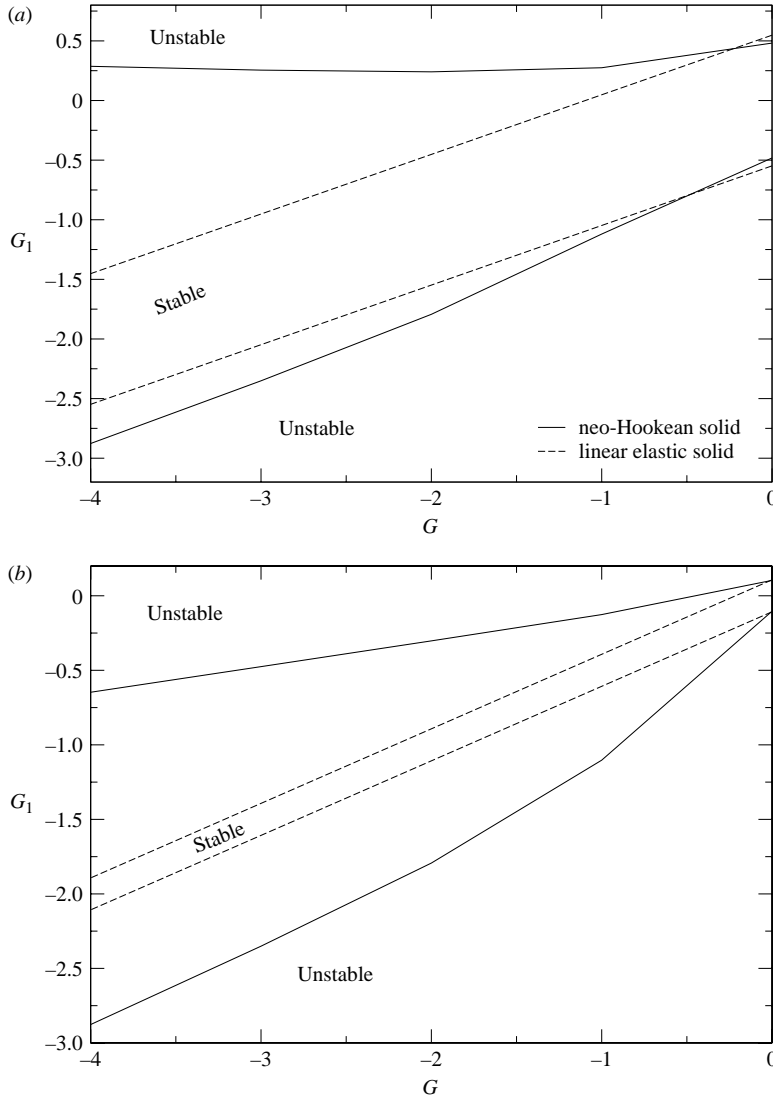


FIGURE 6. Stability windows for combined Couette–Poiseuille flow when  $T = 10$  and (a)  $H = 6$ , (b)  $H = 30$ .

$G_c$  is smaller for a neo-Hookean solid than for a linear elastic solid. This involves examining force balances at the interface, whereas only the continuity of velocity boundary condition was considered in Gkanis & Kumar (2003).

Before proceeding, we briefly consider some simple scaling arguments that can be used to rationalize the behaviour of  $G_c$ . If we recognize that there is a balance between mean shear stresses in the fluid and solid, we have  $\mu_f(\partial v_x/\partial z) \sim E(\partial u_x/\partial z)$  where  $u_x$  is the displacement in the  $x$ -direction in the solid. If we make the order-of-magnitude estimates  $v_x \sim V_w$  and  $u_x, \partial z \sim R$ , then we obtain  $\mu_f V_w/(ER) \sim 1$ . This is consistent with the plateau at low  $H$  observed in figure 4(a). If, on the other hand, we make the estimate that  $\partial z \sim HR$  in the solid (but not the fluid), we obtain  $\mu_f V_w/(ER) \sim H^{-1}$ . This is consistent with the behaviour of  $G_c$  at large values of  $H$ . Although these

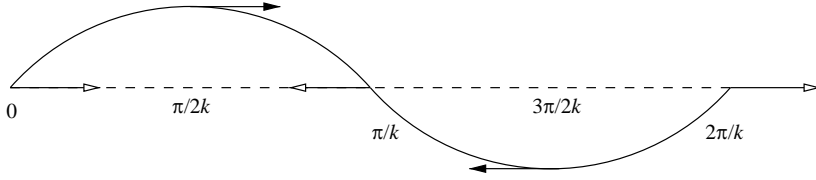


FIGURE 7. Schematic of phase relationships. The solid line shows the vertical position of the perturbed interface and the dashed line shows the location of the unperturbed interface. The solid arrows show the direction of the motion arising from (6.3) and the open arrows show the direction of the force arising from (6.2).

simple arguments cannot explain all of the features of figure 4(a), they do provide a possible interpretation.

Returning to the relative stability of the systems of figure 4(a), we examine the linearized interfacial boundary conditions for the perturbation quantities. This is the natural place to focus since the instability arises owing to the time dependence present in these boundary conditions.

### 6.1. Couette flow past a neo-Hookean solid

The relevant interfacial boundary conditions are:

$$\tau'_{33} - \sigma'_{33} = T \frac{\partial^2 x'_3}{\partial X_1^2}, \quad (6.1)$$

$$\tau'_{31} - \sigma'_{31} = \frac{\partial x'_3}{\partial X_1} (\tau_{11}^o - \sigma_{11}^o) = G^2 \frac{\partial x'_3}{\partial X_1}, \quad (6.2)$$

$$\frac{\partial x'_1}{\partial t} - v'_x = \frac{dv_x^o}{dz} x'_3 = Gx'_3, \quad (6.3)$$

$$\frac{\partial x'_3}{\partial t} - v'_z = 0, \quad (6.4)$$

where the primes denote perturbation quantities and the 'o' denotes base-state values. As in figure 4(a),  $G$  here represents  $G_1$ . The first two boundary conditions are continuity of forces (normal and shear) and the second two boundary conditions are continuity of velocities ( $x$ - and  $z$ -directions).

Equation (6.2) implies that the difference between the shear stress perturbations produces a horizontal force on the interface whose magnitude is equal to the product of  $G^2$  and the local slope. The factor  $G^2$  arises owing to the jump in the base-state values of the first normal stress difference across the interface. If we consider a sinusoidal disturbance, e.g.  $x'_3 = \epsilon \sin(2\pi/k)$ , then this boundary condition yields a force that is  $90^\circ$  out of phase with the vertical position of the interface. Equation (6.3) implies that the difference between the horizontal velocity perturbations is a motion that is in phase with the vertical position of the interface. These relationships are shown in figure 7, where we see that the horizontal force arising from (6.2) tends to compress the crests and extend the valleys. This would tend to have a destabilizing effect, and appears to be similar to what is observed in co-extrusion of two elastic liquids (Hinch, Harris & Rallison 1992). For Couette flow past a linear elastic solid, the right-hand side of (6.2) is zero so this effect is absent. This is consistent with our observation that Couette flow past a neo-Hookean solid is easier to destabilize than Couette flow past a linear elastic solid.

Finally, we note that (6.1) implies that the difference between the normal stress perturbations produces a vertical force on the interface whose magnitude is equal to the product of the interfacial tension and local curvature. With the sinusoidal perturbation given above, this results in a vertical force that is  $180^\circ$  out of phase with the vertical position of the interface. This produces a stabilizing effect, consistent with our observation that  $G_c$  increases as  $T$  increases.

### 6.2. Poiseuille flow in a deformable channel

Equations (6.2) and (6.4) hold for this system, but the other interfacial boundary conditions now have the form:

$$\tau_{33}^o - \sigma_{33}^o = T\kappa - \frac{\partial}{\partial X_3}(\tau_{33}^o - \sigma_{33}^o)x'_3 = T \frac{\partial^2 x'_3}{\partial X_1^2} - G^2 x'_3, \quad (6.5)$$

$$\frac{\partial x'_1}{\partial t} - v'_x = \frac{dv'_x}{dz} x'_3 = -Gx'_3, \quad (6.6)$$

where  $G$  now represents the imposed pressure gradient, which we take to be negative. The only qualitative difference between this system and Couette flow past a neo-Hookean solid is (6.5), where we have the appearance of the term  $-G^2 x'_3$  that arises owing to a jump in the gradient of the base-state normal stresses across the interface. This term represents a force whose magnitude is proportional to  $G^2$ , and it is  $180^\circ$  out of phase with the vertical position of the interface. Therefore, for this system we have another force in addition to interfacial tension that has a stabilizing effect. The critical value of  $G_c$  for this system is thus greater than for Couette flow past a neo-Hookean solid.

### 6.3. Poiseuille flow past a neo-Hookean solid

The interfacial boundary conditions for this system have the form:

$$\tau_{33}^o - \sigma_{33}^o = T\kappa - \frac{\partial}{\partial X_3}(\tau'_{33} - \sigma'_{33})x'_3 = T \frac{\partial^2 x'_3}{\partial X_1^2} - \frac{1}{2}G^2 x'_3, \quad (6.7)$$

$$\tau'_{31} - \sigma'_{31} = \frac{\partial x'_3}{\partial X_1}(\tau'_{11} - \sigma'_{11}) = \frac{1}{4}G^2 \frac{\partial x'_3}{\partial X_1}, \quad (6.8)$$

$$\frac{\partial x'_1}{\partial t} - v'_x = \frac{dv'_x}{dz} x'_3 = -\frac{1}{2}Gx'_3, \quad (6.9)$$

with continuity of velocity in the  $z$ -direction given by (6.4). These boundary conditions will affect the stability of the system in the same way that they did in the previous system. However, because the coefficients are different, the calculated critical imposed strain will be different. In order to make a proper comparison, we set  $b = G/2$  and rewrite (6.7)–(6.9):

$$\tau_{33}^o - \sigma_{33}^o = T\kappa - \frac{\partial}{\partial X_3}(\tau'_{33} - \sigma'_{33})x'_3 = T \frac{\partial^2 x'_3}{\partial X_1^2} - 2b^2 x'_3, \quad (6.10)$$

$$\tau'_{31} - \sigma'_{31} = \frac{\partial x'_3}{\partial X_1}(\tau'_{11} - \sigma'_{11}) = b^2 \frac{\partial x'_3}{\partial X_1}, \quad (6.11)$$

$$\frac{\partial x'_1}{\partial t} - v'_x = \frac{dv'_x}{dz} x'_3 = -bx'_3, \quad (6.12)$$

where  $b$  is taken to be negative. A comparison between (6.10)–(6.12) and (6.2), (6.5) and (6.6) shows that the stabilizing effect of the  $\partial(\tau_{33}^o - \sigma_{33}^o)/\partial X_3$  term is twice as important for Poiseuille flow past a neo-Hookean solid as it is for Poiseuille flow in

a deformable channel. Thus, the critical imposed strain for this system is larger than for Poiseuille flow in a deformable channel. This is seen in figure 4a when  $H > 20$  and  $H < 7$ . The opposite is true when  $7 < H < 20$ , evidently because the two systems enter thin-solid regime at different values of  $H$ .

#### 6.4. Combined Couette–Poiseuille flow

Here, continuity of velocity in the  $z$ -direction is given by (6.4) and the rest of the interfacial boundary conditions are:

$$\tau'_{33} - \sigma'_{33} = T\kappa - \frac{\partial}{\partial X_3}(\tau'_{33} - \sigma'_{33}) x'_3 = T \frac{\partial^2 x'_3}{\partial X_1^2} + \beta G x'_3, \quad (6.13)$$

$$\tau'_{31} - \sigma'_{31} = \frac{\partial x'_3}{\partial X_1} (\tau'_{11} - \sigma'_{11}) = \beta^2 \frac{\partial x'_3}{\partial X_1}, \quad (6.14)$$

$$\frac{\partial x'_1}{\partial t} - v'_x = \frac{dv'_x}{dz} x'_3 = \beta x'_3, \quad (6.15)$$

where  $G$  is taken to be negative. If  $\beta$  is positive, then the term  $\beta G x'_3$  in (6.13) represents a vertical force of magnitude  $\beta G$  which is  $180^\circ$  out of phase with the vertical position of the interface. Hence, it stabilizes the system: an increase in the absolute value of  $G$  causes  $\beta_c$  to obtain larger values (figure 5). In the case of a negative  $\beta$ , the force described by the term  $\beta G x'_3$  in (6.13) is destabilizing. We would therefore expect a decrease in the magnitude of  $G$  to cause a decrease in  $\beta_c$ . However, (6.15) indicates that the  $x$ -component of the velocity of the base state is  $180^\circ$  out of phase with the vertical position of the interface, in contrast to what we have so far observed. Moreover, (6.14) yields a horizontal force that is  $90^\circ$  out of phase with the vertical position of the interface. As a consequence of all these interactions, a decrease in  $G$  causes  $\beta_c$  to decrease for  $H > 2$ , but to increase for  $H < 2$ .

## 7. Conclusions

We have studied the effect of pressure gradients on the stability of creeping flows of Newtonian fluids in channels lined with a neo-Hookean material. Three different configurations were examined with linear stability analysis: (i) Poiseuille flow past a neo-Hookean solid; (ii) Poiseuille flow in a deformable channel; and (iii) combined Couette–Poiseuille flow. In the base state of all of these configurations, there is a first normal stress difference in the solid whose magnitude varies with depth. In the absence of interfacial tension, this gives rise to a short-wave instability. The presence of interfacial tension removes this instability, and for sufficiently thick solids, low-wavenumber modes become unstable first as the applied strain increases above a critical value. For sufficiently thin solids, high-wavenumber modes becomes unstable first instead.

Based on a comparison of the dimensionless critical applied strains, we find that Poiseuille flow past a neo-Hookean solid and Poiseuille flow in a deformable channel are harder to destabilize than Couette flow past a neo-Hookean solid. For combined Couette–Poiseuille flow, the nonlinear elasticity of the solid breaks the symmetry present when a linear elastic model is used, and this leads to two physically distinct critical conditions. This nonlinearity also causes the stability window (the velocities over which the system is stable) to widen as the applied pressure gradient is increased. Much of the above behaviour can be understood by analysing the boundary conditions at the fluid–solid interface. In particular, we find that although jumps in the base-state



normal stresses across the interface have a destabilizing effect for Couette flow past a neo-Hookean solid, they have a stabilizing effect for the Poiseuille flows considered here. Because of the complicated coupling between the base-state quantities and perturbation variables that arises owing to the nonlinear elasticity of the solid, the results presented here could not have been predicted from prior work which used linear elasticity or considered Couette flow past a neo-Hookean solid.

Finally, we comment on the parameter regimes in which the instabilities studied here might be observed in practice. Consider a viscous liquid with  $\mu_f \sim 1$  Pa s, and a plane Couette flow where  $R \sim 10^{-4}$  m and  $V_w \sim 0.1$  m s $^{-1}$ . For relatively thick solids, we require  $G_1 \sim 1$  or less to excite the instability (figure 4a), which implies that we require  $E \sim 10^3$  Pa. These parameters are achievable experimentally, as demonstrated in the studies of Kumaran & Muralikrishnan (2000), Muralikrishnan & Kumaran (2001) and Eggert & Kumar (2004). For relatively thin solids,  $G_1 \sim 10$  is required to excite the instability, meaning that  $E \sim 10^2$  Pa is required. This corresponds to a much softer gel than those used in previous studies and may be difficult to achieve experimentally since such a gel is likely to be rather fragile. For the Poiseuille flows studied here,  $G \sim 1$  or less is required to excite the instability for relatively thick solids. Taking  $R \sim 10^{-4}$  m and  $E \sim 10^3$  Pa, this corresponds to a pressure gradient of  $10^7$  Pa m $^{-1}$ . As this is rather large, the instabilities in the Poiseuille flows studied here will probably be observable only for geometries where the solid thickness is much larger than the fluid thickness.

Acknowledgment is made to the Donors of the The Petroleum Research Fund, administered by the American Chemical Society, for partial support of this research. SK also thanks the Shell Oil Company Foundation for support through its Faculty Career Initiation Funds program, and 3M for a Non-tenured Faculty Award.

## Appendix. Linearized governing equations and boundary conditions

### A.1. Poiseuille flow past a neo-Hookean solid

The governing equations for the fluid are:

$$D\tilde{v}_z + ik\tilde{v}_x = 0, \quad (\text{A } 1)$$

$$-ik\tilde{P}_f + D^2\tilde{v}_x - k^2\tilde{v}_x = 0, \quad (\text{A } 2)$$

$$-D\tilde{P}_f + D^2\tilde{v}_z - k^2\tilde{v}_z = 0, \quad (\text{A } 3)$$

and for the solid:

$$-GD\tilde{x}_3 - ik\tilde{P}_s + (G^2X_3 - \frac{1}{2}G^2)ik\tilde{x}_3 - k^2\tilde{x}_1 + D^2\tilde{x}_1 = 0, \quad (\text{A } 4)$$

$$GD\tilde{x}_1 + ik\tilde{P}_s(GX_3 - \frac{1}{2}G) - (G^2X_3 - \frac{1}{2}G^2)ik\tilde{x}_1 - D\tilde{P}_s - k^2\tilde{x}_3 + D^2\tilde{x}_3 = 0, \quad (\text{A } 5)$$

$$D\tilde{x}_3 + ik\tilde{x}_1 - (GX_3 - \frac{1}{2}G)ik\tilde{x}_3 = 0, \quad (\text{A } 6)$$

where  $D$  is equal to  $\partial/\partial z$  for the fluid and  $\partial/\partial X_3$  for the solid. The boundary conditions at the bottom plate become:

$$\tilde{\mathbf{x}} = \mathbf{0}, \quad (\text{A } 7)$$

and at the top plate:

$$\tilde{\mathbf{v}} = \mathbf{0}. \quad (\text{A } 8)$$

At the interface, we Taylor expand the boundary conditions around  $z = 0$  (the location of the interface in the base state) to obtain:

$$\tilde{v}_z - \alpha \tilde{x}_3 = 0, \quad (\text{A } 9)$$

$$\alpha \tilde{x}_1 - \tilde{v}_x + \frac{1}{2} G \tilde{x}_3 = 0, \quad (\text{A } 10)$$

$$-\frac{1}{4} G^2 i k \tilde{x}_3 + i k \tilde{x}_3 - \frac{1}{2} G D \tilde{x}_3 + D \tilde{x}_1 - i k \tilde{v}_z - D \tilde{v}_x = 0, \quad (\text{A } 11)$$

$$-\tilde{P}_s + 2D \tilde{x}_3 + \tilde{P}_f - 2D \tilde{v}_z + k^2 T \tilde{x}_3 + \frac{1}{2} G^2 \tilde{x}_3 = 0. \quad (\text{A } 12)$$

### A.2. Poiseuille flow in a deformable channel

For the fluid the governing equations simplify to (A 1)–(A 3) and for the solid they take the form:

$$-GD \tilde{x}_3 - i k \tilde{P}_s + G^2 (X_3 - 1) i k \tilde{x}_3 - k^2 \tilde{x}_1 + D^2 \tilde{x}_1 = 0, \quad (\text{A } 13)$$

$$GD \tilde{x}_1 + i k \tilde{P}_s G (X_3 - 1) - G^2 (X_3 - 1) i k \tilde{x}_1 - D \tilde{P}_s - k^2 \tilde{x}_3 + D^2 \tilde{x}_3 = 0, \quad (\text{A } 14)$$

$$D \tilde{x}_3 + i k \tilde{x}_1 - G (X_3 - 1) i k \tilde{x}_3 = 0. \quad (\text{A } 15)$$

At the bottom plate we have the boundary conditions given by (A 7), and at the top plate,  $z = 1$ , we use the following boundary conditions:

$$\tilde{v}_z = 0, \quad (\text{A } 16)$$

$$D \tilde{v}_x = 0. \quad (\text{A } 17)$$

The four interfacial boundary conditions are (A 9), (A 10) without the factor of  $1/2$ , and:

$$-G^2 i k \tilde{x}_3 + i k \tilde{x}_3 - GD \tilde{x}_3 + D \tilde{x}_1 - i k \tilde{v}_z - D \tilde{v}_x = 0, \quad (\text{A } 18)$$

$$-\tilde{P}_s + 2D \tilde{x}_3 + \tilde{P}_f - 2D \tilde{v}_z + k^2 T \tilde{x}_3 + G^2 \tilde{x}_3 = 0. \quad (\text{A } 19)$$

### A.3. Combined Couette–Poiseuille flow

The governing equations for the fluid are (A 1)–(A 3) and for the solid they are:

$$-GD \tilde{x}_3 - i k \tilde{P}_s + G (GX_3 + \beta) i k \tilde{x}_3 - k^2 \tilde{x}_1 + D^2 \tilde{x}_1 = 0, \quad (\text{A } 20)$$

$$GD \tilde{x}_1 + i k \tilde{P}_s (GX_3 + \beta) - G (GX_3 + \beta) i k \tilde{x}_1 - D \tilde{P}_s - k^2 \tilde{x}_3 + D^2 \tilde{x}_3 = 0, \quad (\text{A } 21)$$

$$D \tilde{x}_3 + i k \tilde{x}_1 - (GX_3 + \beta) i k \tilde{x}_3 = 0. \quad (\text{A } 22)$$

The boundary conditions at the bottom and top plate are (A 7) and (A 8), respectively. Taylor expansion of the interfacial boundary conditions around  $z = 0$  transforms the continuity of velocity boundary conditions to (A 9) and (A 10), with  $\beta$  in place of  $G/2$ . Continuity of forces becomes:

$$-i \beta^2 k \tilde{x}_3 + i k \tilde{x}_3 + \beta D \tilde{x}_3 + D \tilde{x}_1 - i k \tilde{v}_z - D \tilde{v}_x = 0, \quad (\text{A } 23)$$

$$-\tilde{P}_s + 2D \tilde{x}_3 + \tilde{P}_f - 2D \tilde{v}_z + k^2 T \tilde{x}_3 - \beta G \tilde{x}_3 = 0. \quad (\text{A } 24)$$

## REFERENCES

- CARPENTER, P. W., LUCEY, A. D. & DAVIES, C. 2001 Progress on the use of compliant walls for laminar flow control. *J. Aircraft* **38**, 504–512.
- CHEN, K. 1991 Elastic instability of the interface in Couette flow of viscoelastic liquids. *J. Non-Newtonian Fluid Mech.* **40**, 261–267.
- DAVEY, A. 1973 A simple numerical method for solving Orr–Sommerfeld problems. *Q. J. Mech. Appl. Maths* **26**, 401–411.
- DAVIES, C. & CARPENTER, P. W. 1997 Instabilities in plane channel flow between compliant walls. *J. Fluid Mech.* **352**, 205–243.

- EGGERT, M. D. & KUMAR, S. 2004 Observations of instability, hysteresis, and oscillation in low-Reynolds-number flow past polymer gels. *J. Colloid Interface Sci.* **278**, 234–242.
- GAD-EL-HAK, M. 2003 Drag reduction using compliant walls. In *Flow past Highly Compliant Boundaries and in Collapsible Tubes* (ed. P. W. Carpenter & T. J. Pedley). Kluwer.
- GKANIS, V. & KUMAR, S. 2003 Instability of creeping Couette flow past a neo-Hookean solid. *Phys. Fluids* **15**, 2864–2471.
- GORODTSOV, V. A. & LEONOV, A. I. 1967 On a linear instability of plane parallel Couette flow of viscoelastic fluid. *J. Appl. Math. Mech.* **31**, 310–319.
- HAMADICHE, M. & GAD-EL-HAK, M. 2002 Temporal stability of flow through viscoelastic tubes. *J. Fluids Struct.* **16**, 331–359.
- HINCH, E. J., HARRIS, O. J. & RALLISON, J. M. 1992 The instability mechanism for two elastic liquids being co-extruded. *J. Non-Newtonian Fluid Mech.* **43**, 311–324.
- HO, T. C. & DENN, M. M. 1977 Stability of plane Poiseuille flow of a highly elastic liquid. *J. Non-Newtonian Fluid Mech.* **3**, 179–195.
- KRINDEL, P. & SILBERBERG, A. 1979 Flow through gel-walled tubes. *J. Colloid Interface Sci.* **71**, 39–50.
- KUMARAN, V. 1995 Stability of the viscous flow of a fluid through a flexible tube. *J. Fluid Mech.* **294**, 259–281.
- KUMARAN, V. 1998 Stability of fluid flow through a flexible tube at intermediate Reynolds number. *J. Fluid Mech.* **357**, 123–140.
- KUMARAN, V., FREDRICKSON, G. H. & PINCUS, P. 1994 Flow-induced instability at the interface between a fluid and a gel at low Reynolds number. *J. Phys. Paris II* **4**, 893–911.
- KUMARAN, V. & MURALIKRISHNAN, R. 2000 Spontaneous growth of fluctuations in the viscous flow of a fluid past a soft interface. *Phys. Rev. Lett.* **84**, 3310–3313.
- MACK, L. M. 1976 A numerical study of the temporal eigenvalue spectrum of the Blasius boundary layer. *J. Fluid Mech.* **73**, 497–520.
- MACOSKO, C. W. 1994 *Rheology: Principles, Measurements, and Applications*. Wiley-VCH.
- MALVERN, L. E. 1969 *Introduction to the Mechanics of a Continuous Medium*. Prentice-Hall.
- MORIARTY, J. A. & GROTBORG, J. B. 1999 Flow-induced instabilities of a mucus–serous bilayer. *J. Fluid Mech.* **397**, 1–22.
- MURALIKRISHNAN, R. & KUMARAN, V. 2001 Experimental study of the instability of the viscous flow past a flexible surface. *Phys. Fluids* **14**, 775–780.
- PIERUCCI, M. & MORALES, P. G. 1990 Effect of finite thickness flexible boundary upon the stability of a Poiseuille flow. *Trans. ASME: J. Appl. Mech.* **57**, 1056–1060.
- RENARDY, Y. 1988 Stability of the interface in two-layer Couette flow of upper convected Maxwell liquids. *J. Non-Newtonian Fluid Mech.* **28**, 99–115.
- SHANKAR, V. & KUMAR, S. 2003 Instability of viscoelastic plane Couette flow past a deformable wall. *J. Non-Newtonian Fluid Mech.* **116**, 371–393.
- SHANKAR, V. & KUMARAN, V. 2000 Stability of fluid flow in a flexible tube to non-axisymmetric disturbances. *J. Fluid Mech.* **407**, 291–314.
- SHANKAR, V. & KUMARAN, V. 2001 Weakly nonlinear stability of viscous flow past a flexible surface. *J. Fluid Mech.* **434**, 337–354.
- SRIVATSAN, L. & KUMARAN, V. 1997 Flow-induced instability at the interface between a fluid and a gel. *J. Phys. Paris II* **7**, 947–963.